A DIVE INTO THEORETICAL HEAT FLUX OF DIFFUSE FLOW HYDROTHERMAL VENT PLUMES AND APPLICATIONS TO EXTRATERRESTRIAL OCEANS

By

JESSE H. NOBLE

A thesis submitted to the

School of Graduate Studies

Rutgers, The State University of New Jersey

In partial fulfillment of the requirements

For the degree of

Master of Science

Graduate Program in Oceanography

Written under the direction of

Karen Bemis

And approved by

_____

_____

_____

New Brunswick, New Jersey

October 2024

ABSTRACT OF THE THESIS

A Dive into Theoretical Heat Flux of Diffuse Flow Hydrothermal Vent Plumes and Applications to Extraterrestrial Oceans

by JESSE H. NOBLE

Thesis Directors:

Karen Bemis

“Diffuse flow” is a general term for slow-moving, low temperature (0.2 °C to ~100 °C) fluids discharged from small cracks around hydrothermal vent systems. Sea water is heated up by subsurface magma, inducing a vertical movement. Using the remotely operated vehicle JASON, the vertical velocities of the plume heads discharging at the seafloor and their temperatures were measured at Axial Seamount, ASHES vent field in the eastern Pacific between the years 2018 - 2019. This was done to compare *in situ* samples with Cabled Array Vent Imaging Sonar (COVIS) data to estimate a total heat flux from diffuse flow vents. Observed vertical velocities are determined by tracking plume head rise from video particle-tracking analysis, and heat fluxes were calculated using 1- and 2-meter-tall thermistor arrays. The maximum temperatures were utilized from each position on the arrays for six distinct plume sites, averaging from top of array to vent opening 3.06 °C - 13.77 °C for the 2019 sites and 3.38 °C - 8.68 °C for the 2018 sites. The height on the array corresponds to the distance of the thermistor from the vent's orifice, the closer the thermistor, the lower the height. This approach proved more precise than relying on the mean temperatures, given the variability introduced by the movement of the arrays and turbulence around plumes. The vertical velocities of each plume head were calculated by segmenting the video footage into frames of either 0.5 or 1 second increments and tracking particle trajectory throughout each frame. Geological reference points were employed to stabilize the background, mitigating movement induced by shifting video frames. The mean vertical velocity across the nine tracked plume heads is approximately 0.08 m/s. The integration of thermistor array data with vertical velocities allows for estimating the total heat flux for the seawater above seven vent openings. Additionally, the investigation into diffuse flow vents offers valuable insights into postulating the plausible environmental conditions found on exoplanets hosting hydrothermal vent systems. A subsequent phase of this

research will entail using velocity and temperature data gathered from ASHES vent field to infer potential conditions, including an idea of heat dispersion, around hypothetical hydrothermal vents beneath Enceladus' icy crust. This component is essential for the exploration aimed at uncovering life on celestial bodies outside of our planet.

ACKNOWLEDGEMENTS

I would like to dedicate this research to my pop who inspired me to be curious about the natural world and explore. Thank you to all my family and friends for listening patiently while I talked their ears off about my research. Thank you to my advisors for providing me with support throughout this project. Last but not least, thank you to my dogs Marlo and Harley for providing me with good company as I wrote this.

Thank you for support from the NSF grant OCE 1736702 awarded to principal investigator Karen Bemis.

Contents

LIST OF FIGURES

1. Introduction

1.1 Other Studies

Despite extensive observations of hydrothermal vent fields, quantifications of heat circulation and the heat it transports are limited. A variety of methods for estimating the discharge velocities of hydrothermal fluids and calculating heat flux have been used at ASHES field vents. Rona and Trivett (1992) obtained a total diffuse heat transfer of 15 - 75 $\times$ 10^6W from individual vents in ASHES vent field by calculating with a standard plume model based on a grid of temperature measurements at varying altitudes taken by sensors attached to the D.S.V *Alvin*. Vertical velocities were obtained by tracking individual particles around the vents. MacDonald et al. (1980) calculated heat transfer from vents located on the East Pacific Rise using temperature, velocity, and vent radius measurements made at the discharge site. The equation employed to calculate heat transfer in this paper was also utilized in this research to determine heat flux. Methods of vent analysis were taken from Bemis (2022) and adapted.

1.2 Diffuse Flow versus Black Smokers

Hydrothermal vent systems form when magma heats subsurface fluids, which then escape through the seafloor (Fisher et al. 2007). There are two types of flow for these vent systems: black smokers and diffuse flow. Black smoker vents are high momentum plumes caused by the drastic heating of seawater, averaging around 250 °C to 350 °C (Bemis et al. 2019). The focused vent geometry acts as a streamline for the vent fluids when exiting, sustaining the velocity of the flow. The dark, smoky coloration of the jets are from the precipitation of iron-sulfide, which also creates chimneys around the vent openings. These vents are directly above magma chambers located several kilometers beneath the seafloor (Joseph 2023). The main difference between black smoker hydrothermal vents and diffuse flow vents is the chemical composition of the vent water and their orifice geometries. Black smoker vent water exists with minimal modification while diffuse flow vent water mixes with the seawater near the opening of the vents. Diffuse flow vent geometries range from small cracks to small mounds of sulfide. Due to the nature of the geometries, subsurface waters mix with downwelling seawater causing resistance (seawater flowing in, diffuse flow going out) resulting in lower velocities and temperatures (Joseph 2023). Unlike the black smokers, diffuse flow vents emit much cooler temperatures ranging from 0.2 °C to ~100 °C (Bemis et al. 2019).

1.3 ASHES Vent Field

The ASHES vent field is located at approximately 130.01° W, 45.93° N (see Figure 1) within the Axial Seamount on the Juan de Fuca Ridge (Butterfield et al. 1990). The vent field is about a 150 m^2 box containing four to five main black smoker chimneys and multiple diffuse flow sites with high porosity (Gilbert et al. 2007). This study looks at 6 different diffuse flow sites from varying areas around the vent field. Measurements at some sites were repeated either by looking at varying segments of the same particle plume or from two separate times the site was visited. Many different studies have been conducted at this vent field including the ones by Butterfield et al. (1990) on the chemical composition of vent fluids and Xu et al. (2021) on using acoustic backscattering from COVIS to monitor vent discharge. COVIS is the Cabled Array Vent Imaging Sonar that measures long term hydrothermal vent emissions.

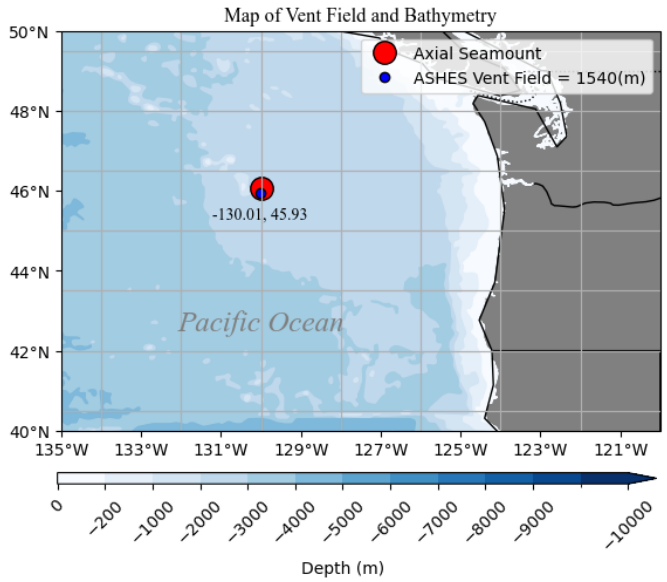

Figure 1: This is a map showing the coordinates of ASHES vent field (130.01 °W, 45.93 °N) located in the Pacific Ocean with an average depth of about 1540-m. The color bar at the bottom indicates bathymetry. The bathymetry data was taken from an open-source site, "Natural Earth" (https://www.naturalearthdata.com/downloads/10m-physical-vectors/10m-bathymetry/).

1.4 Comparison of Video Data Heat Flux with COVIS Measurements

Hydrothermal vents serve as an oasis for life in the deep ocean, thriving in an environment where light cannot penetrate, and conditions are extreme. They provide a significant source of heat and nutrients to the deep ocean essential for the growth and survival of these communities (German et al. 2016). Tracking the circulation through movement and dispersions of the vent plumes provides us with an insight as to how heat and nutrients are being dispersed in this environment. These vents release nutrients crucial for the survival of life on Earth, and it is theorized that life on our planet may have originated around them (Martin et al. 2008). This theory allows us to explore the concept of applying knowledge about hydrothermal vent systems on Earth to the search for potential life on extraterrestrial bodies in our solar system. There are gaps in the knowledge surrounding the geological and mechanical aspects of diffuse flow vents which this study aims to learn more about. By comparing calculations of heat flux from the diffuse flow vents with COVIS data, we can confirm accuracy of measured vertical velocities

through the methods used for this research. This paper will overview the methodology used for this research, the results for temperature, velocity, and heat flux measurements over the diffuse flow sites, and a review of relevant outside literature to relate extraterrestrial hydrothermal vents to vents on Earth using an analog for what heat circulation might look like.

2. Methodology

Diffuse flow vents play a vital role in facilitating heat and nutrient circulation within the bathypelagic zone, thus significantly impacting our comprehension of the biological and physical dynamics dependent on these vents. The goal for this research was to extrapolate *in situ* vertical velocities from diffuse flow vents to compare with heat flux maps from acoustic backscattering data collected by COVIS. The COVIS data was pulled from Jackson et al. (2022) and used to compare the heat flux of the specific areas around the vent field in which the meter stick was used to obtain flow rates. This analysis was conducted to obtain a level of accuracy in flow rates using heat flux calculations for the diffuse flow vents. Another objective for the research was to estimate temperature values from thermistor arrays to help calculate heat flux of the plume water. In this chapter, we will discuss the process and equipment used to obtain the data, analyze the results, and discuss what we can infer from the outcomes of this research and how it relates to outside literature.

There was a variety of different instrumentation used for this project. Woods Hole Oceanographic Institute deployed an ROV called JASON that carried a basket of equipment down to the sea floor with it, using its robotic arms to grab and maneuver temperature probes and meter sticks calibrated with 5-cm increments used to measure the plume head distances. It is important to note that the use of flowmeters was attempted to measure the vertical velocities from the vents, however the flow was not strong enough to provide results. Thermistor arrays were used to measure the change in temperatures from the mouth of the vents and upward. In 2018, 1-meter-tall thermistor arrays were used with 5 levels of varying increments to them (see Figure 2 for heights). In 2019, 2-meter-tall arrays were used with 10 increment levels increasing in height from the bottom.

The particle plume head data was originally collected in the form of videos from high-definition cameras attached to the ROV JASON by poking around the orifices of diffuse flow vents and disturbing sediment. For analysis purposes

it is worth noting while filming these videos the frames were not always stable due to the rocking of the ROV and the camera angle was not always exactly head on. Using the video data, we identified a useful section of video and clipped it to just that section (when the sediment started rising to when it exited the screen). Once the video is clipped, the lengths were only a few seconds long, so the frames were extracted by either the second or half seconds. To extract the frames, we used Python code to set an output directory and then looped through the frames to save as JPEGs. Using the individual frames, we then switched over to MATLAB to use code that allows the user to select individual points on each frame. There are two categories of selected points: stabilization which selects for stationary geological features in the same place for each frame to stabilize any movement from the camera that may have occurred frame by frame and plume head tracking in which 15-20 points are selected in each frame outlining the plume head, following the sediment as the plume pushes it. Using the manually selected points, we created a time series figure showing the selected points for the plume head connected and colored by frame which gives us the final product (shown in Figure 4). Distances were scaled using the meter stick located next to the vent openings in each video, which allowed calculation of velocities in relevant units (meters/second).

The thermistor array data was originally collected using JASON mechanical arms to move arrays around each vent site, placing the arrays over the openings of diffuse flow vents. The data was uploaded for each individual array and the time series was plotted using Python. The data was then sliced down to the exact times that each individual array was over a vent in the same site as the video was taken. The mean temperatures and maximum temperatures were then taken from each array height for each vent. In this research, the maximum temperature from each site will be used as it was determined that due to turbulence around the vent openings, these would provide the most accurate calculations.

Diffuse flow vents are a type of heat-buoyancy driven plume, meaning their momentum is dependent on the temperature change of the surrounding water. The warmer water heated from the orifice of the diffuse flow vent is more buoyant than the cooler bottom water, causing a vertical movement of the warmer vent water (Papanicolaou and List 1987). Horizontal currents or other turbulent related disturbances interfere with the flow once the plume exits the vent orifice, making calculating the vertical velocities of diffuse flow vents difficult. Plume theory is a set of assumptions used to predict vertical velocities above diffuse flow sources based on assumptions of vent level

buoyancy and heat flux. Simple plume theory allows for an assumption of purely vertical flow to simplify the process in consideration of a temporally averaged plume. A centerline is taken of the plume trajectory and the units of velocity, momentum, buoyancy and heat are assessed to derive a relationship between vertical velocity (which is measured) and buoyancy flux. The equation is as follows:

$$\mathbf{w = b\,(B/z)^{1/3}}$$

where **w** is the vertical velocity on the centerline, **b** is the empirical constant and **B** is the initial vent buoyancy flux. The buoyancy flux can be either estimated from the coefficient of thermal expansion, acceleration of gravity, change in temperature, and volume flux or by rearranging the equation above (Bemis 2022).

Heat flux was measured for each individual vent using the heat transfer equation:

$$\mathbf{H_m = \pi r^2 v \rho C_p \Delta T}$$

used in MacDonald et al. (1980). The heat transfer for the measured vent area was found using an estimated radius of the orifices, the measured velocities, and the temperature changes. $\mathbf{H_m}$ being heat transfer, $\boldsymbol{\pi r^2}$ being the measured area, **v** as the average velocity, **ρ** as average density, $\mathbf{C_p}$ as the heat capacity, and **ΔT** being the temperature change. The measured heat transfer was then used in the equation:

$$\mathbf{H_c = (H_m \times A_c) / A_m}$$

to solve for $\mathbf{H_c}$ which is the heat transfer of an entire crack instead of just the point source. $\mathbf{A_c}$ and $\mathbf{A_m}$ are areas of the crack and measured point source. The heat transfer for the area of the cracks in a 1-m^2 box area around the point source is then used to calculate the heat flux within the box. The equation for heat flux is as follows:

$$\mathbf{P_T = P_c / A_{box}}$$

with $\mathbf{P_T}$ being the total heat flux of the 1-m^2 box, $\mathbf{P_c}$ being the heat flux of the cracks, and $\mathbf{A_{box}}$ being the area of the box (1-m^2). The heat flux data will be analyzed by comparing the calculated with COVIS data. The COVIS data is shown in 1-m^2 boxes colored by the estimated heat flux during a specific time.

3. Results

The maximum temperature for each vent site on each array position was taken to obtain a total heat flux for the measured vents (see Figure 2). For 2019 the thermistor arrays (6,7) had 10 temperature sensors attached at varying height from the bottom at 1-cm above the vent orifice to 190-cm. The 1H site had a maximum temperature of 14.39 °C at 1-cm and a maximum temperature of 2.97 °C at 190-cm. The 3B site at 1-cm had a maximum temperature of 13.15 °C and at 190-cm 3.14 °C. The 2019 vent sites had overall higher temperatures than the 2018 sites. The 2018 thermistor arrays (1,2) had 5 temperature sensors attached in heights starting at 0.98-cm from the vent orifice to 31.28-cm at the top. The 1F site had the lowest maximum temperatures with 3.42 °C at 0.98-cm and 2.42 °C at 31.28-cm. Site 1D had the highest maximum temperature at 0.98-cm with 17.15 °C and dipped down to 3.50 °C at 31.28-cm. Site 1B started with 5.94 °C at 0.98-cm and did not see much change with 4.03 °C at 31.28-cm. Site 2G at 0.98-cm was 8.37 °C and 3.66 °C at 31.28-cm. All sites saw a decrease in temperature from the bottom temperature sensor to the fifth temperature sensor and for the 2019 sites, there was a steady decrease from the fifth to top.

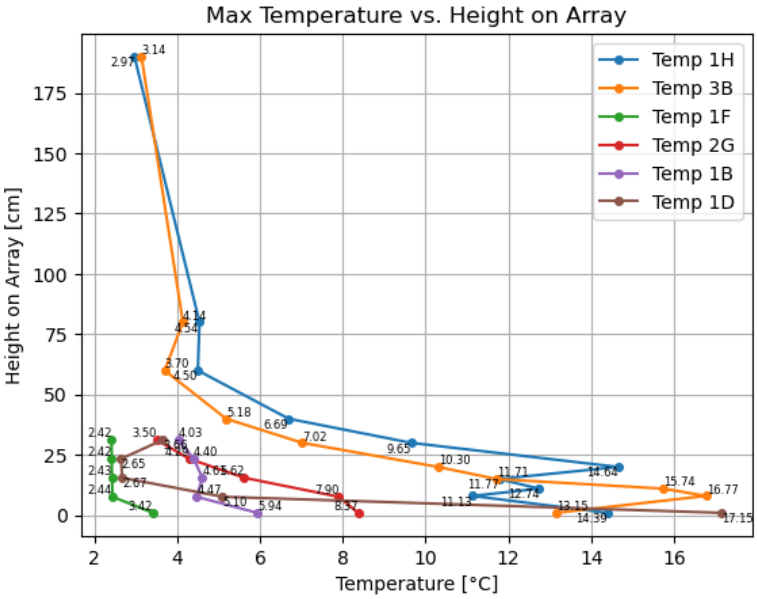

Figure 2: The maximum temperatures from each site are shown corresponding with the height for each thermistor on the arrays. The data was filtered to display only the time intervals when the array was positioned at a diffuse flow vent across each of the six sites. The 2019 data (sites 1H and 3B) used a 2-meter-tall array while the 2018 sites (1F, 2G, 1B, and 1D) used 1-meter-tall arrays.

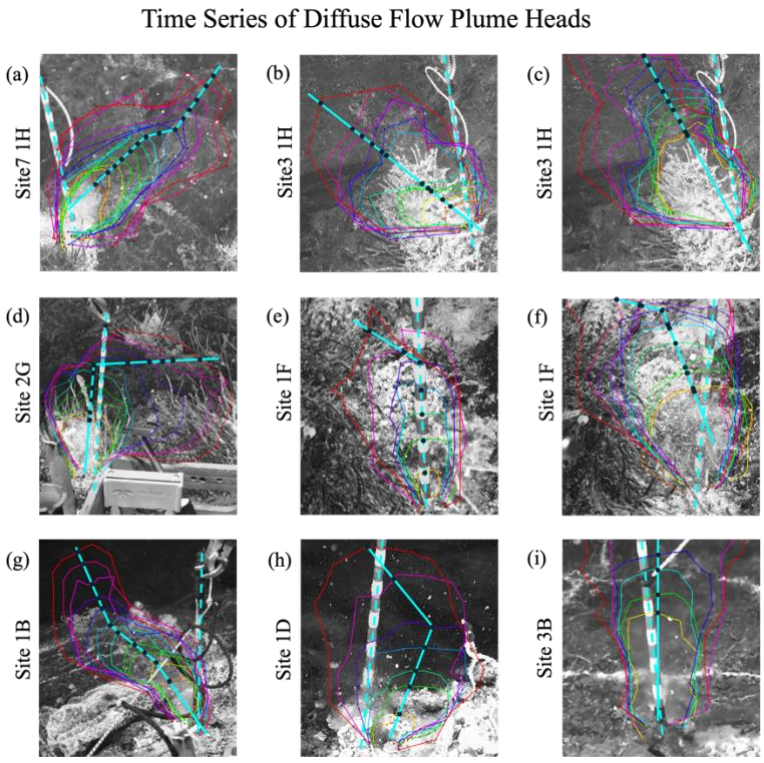

Figure 3: Depiction of the nine plume heads tracked over time sorted by their respective sites, starting from orange or yellow line and ending on red. The cyan dotted lines indicate the position of the measuring stick and the center lines for the plume trajectories. Some plumes change trajectories throughout the course of time resulting in more than one segment for the centerlines. Plumes (a)-(c) and (i) are from 2019 and (d)-(h) are 2018. The plumes measured by one second increments are (a)-(e) and plumes measured by ½ second increments are (f)-(i).

The velocities were found using the solid cyan line and black markers in Figure 3, which is the center lines of the plumes and the selected spot where the center line crosses the time intervals. Vertical velocities for each plume head taken from the video data were calculated and plotted in a velocity versus time graph to compare the different sites in Figure 4. The sites are not the same time lengths due to the nature of the videos and how much was captured of the sediment rising. Site 2G exhibited the slowest average vertical velocities, as shown in the plot where these velocities decrease significantly towards the last few timestamps. Conversely, Site 1D had the fastest velocities, which corresponded with the high initial temperatures. In a steady state environment, the vertical velocities should start faster and then decrease over time, however, in this environment there are a lot of outside factors affecting the trajectory of the plumes. It is to be expected that turbulence around the plumes would affect the vertical velocities due to the weaker nature of the flow.

Heat flux was calculated from the temperatures and vertical velocities for each of the nine plumes in Figure 3. Site 3B shown in Figure 3 image (i) had the greatest calculated heat flux coming out to 0.509 ± 0.05 MW/m^2, lining up with the 2019 COVIS data from Jackson et al. (2022) which was around 0.500 MW/m^2. Site 1F shown in Figure 3 images (e and f) had the lowest calculated heat flux 0.008 MW/m^2. This calculation could not be compared with the COVIS data because Site 1F located in a shadow caused by the black smoker chimney known as Mushroom. Site 7-1H Figure 3 image (a) had a calculated heat flux of 0.100 ± 0.02 MW/m^2 with the corresponding COVIS data of 0.100 MW/m^2. At Site 3-1H Figure 3 image (b and c), the calculated heat flux was 0.115 ± 0.02 MW/m^2, compared to the COVIS data of 0.100 MW/m^2. At Site 2G Figure 3 image (d), the calculated heat flux was 0.052 ± 0.01 MW/m^2, with COVIS data showing 0.050 MW/m^2. At Site 1B Figure 3 image (g), the calculated heat flux was 0.055 ± 0.01 MW/m^2, whereas the COVIS data indicated around 0.100 MW/m^2. At Site 1D Figure 3 image (h), the calculated heat flux was 0.181 ± 0.05 MW/m^2, while the COVIS data recorded 0.250 MW/m^2. The overall average difference between the calculated heat flux and COVIS heat flux is around ± 0.023 MW/m^2.

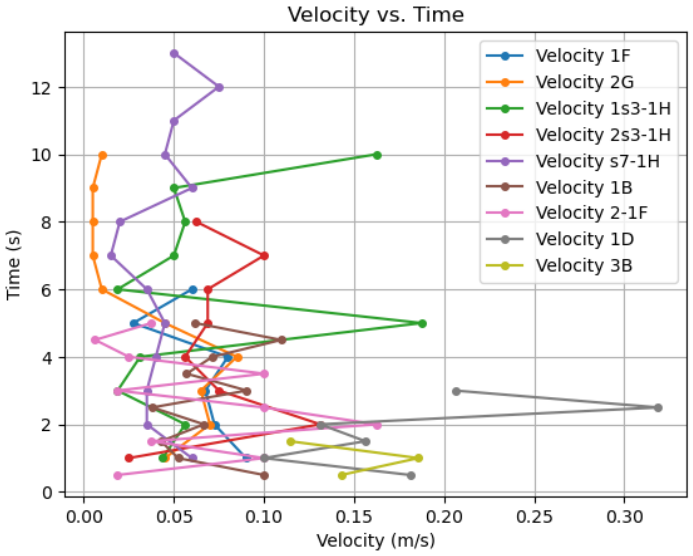

Figure 4: Average vertical velocities are as follow: (s7-1H) 0.0438 m/s, (1s-1H) 0.0675 m/s, (2s3-1H) 0.0649 m/s, (2G) 0.0345 m/s, (1F) 0.0663 m/s, (2-1F) 0.0606 m/s, (1B) 0.0691 m/s, (1D) 0.1604 m/s, (3B) 0.1476 m/s.

4. Discussion

The turbulence around the vents could be caused by multiple factors such as disturbance from the movement of the ROV, horizontal bottom velocities, or counter flow of seawater seeping into the diffuse flow vents. A study by Scheirer et al. (2006) found that temperature and flow variability near diffuse flow vents to be connected to the near-bottom currents through tidal and inertial forcing. This turbulence is the reason our results for the vertical velocities and temperatures are not as we expect to see with the steady state. Looking back at the temperature curves in Figure 2, the recorded temperatures from 2019 exhibit turbulence close to the opening of the vents from the zig zag pattern

within the first 25-cm. After this there is a somewhat uniform curve that would be expected in a steady state environment. The 2018 temperatures are more uniform, but still exhibit some turbulence around the bottom. Looking at the data, there does not seem to be a direct correlation between temperature and velocity. Site 2G with the lowest average velocity has an average starting temperature. Site 1H which had the second highest starting temperature has average or below average vertical velocities. This discrepancy can be attributed to both the positioning of the thermistor arrays over the vent orifices and the turbulence around the vents since the relationship between velocity and temperature requires a steady state. The heat flux calculations from the video data matched the heat flux from COVIS data with statistical significance. The average percent error for the 6 different vent sites compared with COVIS was about 16 %. Due to the limitation of viewing the vent systems through video imaging, the areas used for the heat flux calculations may differ slightly from the true areas. The camera angle of the video introduced errors in calculating the vertical velocities of the vent because the camera was not positioned at a 0° angle to the horizontal. A percent error for this was calculated by solving for the vertical velocities over larger time differences (3 time increments instead of 1). The average percent error for the 9 different camera angles was around 6 %. Some of the limitation for this research stems from the fact that the data used was collected before the idea for this thesis came about so there were only a few segments that were usable for the type of plume head tracking done. Along with this, deep sea research is always limited to some degree by what you can use to collect data and how accurate that method is.

Data collection is not only a limiting factor for deep-sea research; it also restricts the search for life on other planets. Our current technological capabilities constrain the extent to which we can gather viable data for these explorations. Given our limited knowledge of extraterrestrial oceans within our solar system, determining their physical conditions is challenging. One objective of this research, if it were to continue, is to use the collected data as an analog for deep-sea heat circulation on extraterrestrial bodies harboring oceans. The study by Bire et al. (2023) discusses the oceanic conditions of Enceladus and Europa, two of the icy moons in our solar system, and explores how hydrothermal vent plumes behave in these environments. Enceladus is assumed to have a fresher ocean than Earth and therefore the combination of heat and chemicals from the vent water make the plumes rise more easily due to the lower density of the surrounding waters. The plumes would spread more rapidly and widely leading to a greater distribution of heat and nutrients essential for life. Given the greater buoyancy of the vent waters, it can be

inferred that vertical velocities would be higher in similar vent systems on Enceladus compared to those recorded on Earth in this study. Comparatively, Europa has saltier waters and therefore exhibits slower rising plumes due to the higher density of surrounding waters.

5. Conclusion

There are multiple things in this research that could be improved upon for an overall better accuracy in the calculated numbers. Tracking the plume heads was performed visually, and although the human eye is quite reliable, developing an AI program to digitally track plume head trajectories would slightly reduce the associated human error. The camera angle adds in a degree of error as well when calculating the vertical velocity. This method could also cut figure production time down as the current method is tedious and inefficient. If this research was to be done over again, the temperature measurements would be collected using the arrays at similar times the vertical velocities were measured instead of using mean temperatures collected from different time periods around the ASHES vent field. In addition, different camera angles designed for the experiment would be used to reduce error as well as repeating takes. Using the method for tracking particles would also result in more video footage from various sites, as this would be a primary objective for the current visit. This would give a larger sample size for the vertical velocities and could give a better estimate of total heat flux from the diffuse flow vents. This research could provide insights into the total heat flux and flow rates of individual theoretical vents on Enceladus and other extraterrestrial oceans. To address this, we should compare the differences in conditions and analyze how these variations would impact various factors.

REFERENCES

Bemis, K. G. (2022), Understanding the Physical Dynamics of Diffuse Discharge Plume, abstract OS45D-1231 presented at 2022 AGU Fall Meeting, 12-16 Dec.

Bemis, K., Lowell, R. P., & Farough, A. (2019). *Diffuse Flow On and Around Hydrothermal Vents at Mid-Ocean Ridges*. Oceanography. http://www.tos.org/oceanography

Bire, S., Mittal, T., Kang, W., Ramadhan, A., Tuckman, P., German, C. R., Thurnherr, A. M., & Marshall, J. C. (2023). Divergent Behavior of Hydrothermal Plumes in Fresh versus Salty Icy Ocean Worlds. https://doi.org/10.22541/essoar.167397346.61500980/v1

Butterfield, D. A., Massoth, G. J., McDuff, R. E., Lupton, J. E., & Lilley, M. D. (1990). Geochemistry of hydrothermal fluids from axial seamount hydrothermal emissions study vent field, Juan de Fuca Ridge: Subseafloor boiling and subsequent fluid-rock interaction. Journal of Geophysical Research: Solid Earth, 95(B8), 12895–12921. https://doi.org/10.1029/jb095ib08p12895

Fisher, C., Takai, K., & Le Bris, N. (2007). Hydrothermal Vent Ecosystems. Oceanography, 20(1), 14–23. https://doi.org/10.5670/oceanog.2007.75

German, C. R., Casciotti, K. A., Dutay, J.-C., Heimbürger, L. E., Jenkins, W. J., Measures, C. I., Mills, R. A., Obata, H., Schlitzer, R., Tagliabue, A., Turner, D. R., & Whitby, H. (2016). Hydrothermal impacts on trace element and isotope ocean biogeochemistry. Philosophical Transactions of the Royal Society A: Mathematical, Physical and Engineering Sciences, 374(2081), 20160035. https://doi.org/10.1098/rsta.2016.0035

Gilbert, L. A., McDuff, R. E., & Johnson, H. P. (2007, January 1). Porosity of the upper edifice of Axial Seamount. Geology. https://doi.org/10.1130/G22892A.1

Jackson, D., Bemis, K., Xu, G., & Ivakin, A. (2022). Sonar observation of heat flux of diffuse hydrothermal flows. Earth and Space Science, 9(10). https://doi.org/10.1029/2021ea001974

Joseph, A. (2023). Terrestrial analogs & submarine hydrothermal vents—their roles in exploring Ocean Worlds, habitability, and life beyond earth. Water Worlds in the Solar System, 311–358. https://doi.org/10.1016/b978-0-323-95717-5.00012-8

Macdonald, K. C., Becker, K., Spiess, F. N., & Ballard, R. D. (1980). Hydrothermal heat flux of the “Black Smoker” vents on the East Pacific Rise. Earth and Planetary Science Letters, 48(1), 1–7. https://doi.org/10.1016/0012-821x(80)90163-6

Martin, W., Baross, J., Kelley, D. et al. Hydrothermal vents and the origin of life. Nat Rev Microbiol 6, 805–814 (2008). https://doi.org/10.1038/nrmicro1991

Papanicolaou, P. N., & List, E. J. (1987). Statistical and spectral properties of tracer concentration in round buoyant jets. International Journal of Heat and Mass Transfer, 30(10), 2059–2071. https://doi.org/10.1016/0017-9310(87)90086-x

Rona, P. A., & Trivett, D. A. (1992). Discrete and diffuse heat transfer at ashes vent field, axial volcano, Juan de Fuca Ridge. Earth and Planetary Science Letters, 109(1–2), 57–71. https://doi.org/10.1016/0012-821x(92)90074-6

Scheirer, D. S., Shank, T. M., & Fornari, D. J. (2006). Temperature variations at diffuse and focused flow hydrothermal vent sites along the northern East Pacific Rise. Geochemistry, Geophysics, Geosystems, 7(3). https://doi.org/10.1029/2005gc001094

Xu, G., Bemis, K., Jackson, D., & Ivakin, A. (2021). Acoustic and in-situ observations of deep seafloor hydrothermal discharge: An Ooi cabled array Ashes Vent field case study. Earth and Space Science, 8(3). https://doi.org/10.1029/2020ea001269

SUPPLEMENTARY FIGURES

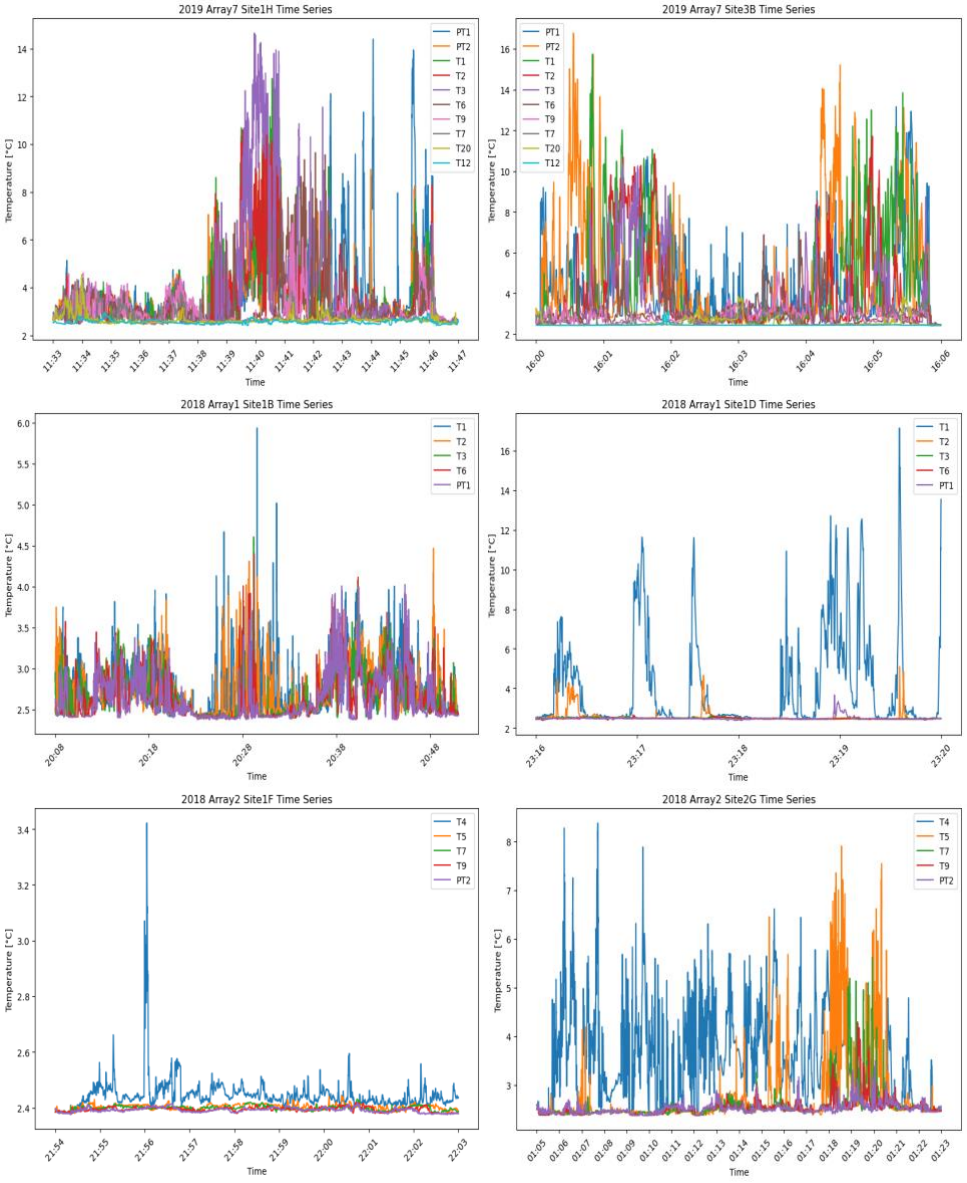

Figure S 1: Depiction of thermistor array full time series from six different vent sites at ASHES vent field. Sites 1H and 3B were taken in 2019 and sites 1B, 1D, 1F, and 2G were taken in 2018. The time is shown in hours/minutes of when the arrays were placed over the observed vents. The labels for the arrays are ordered from closest to farthest from the vent orifice.

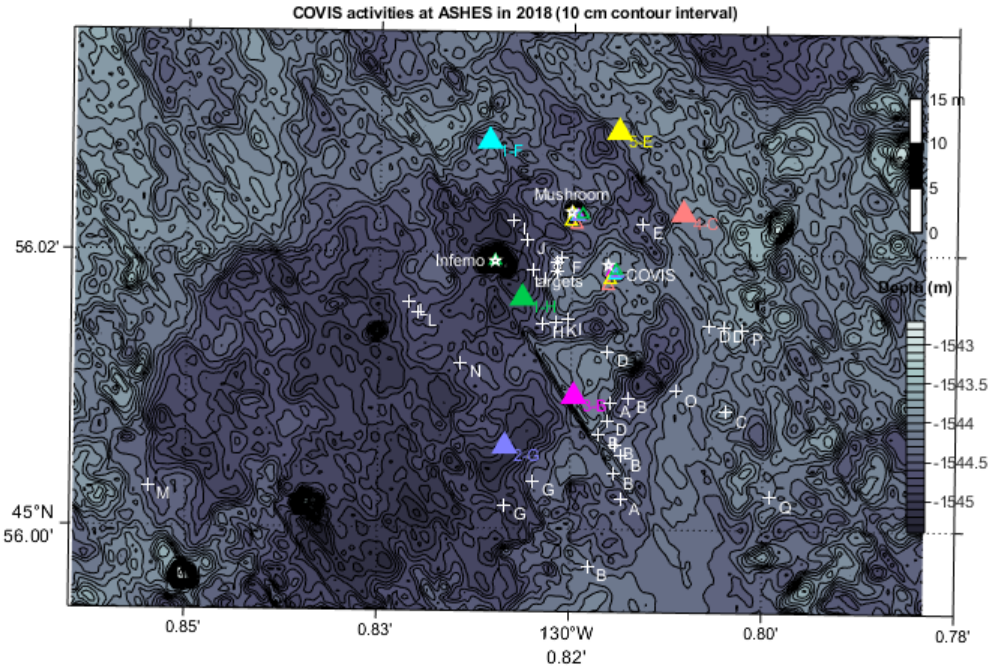

Figure S 2: This figure depicts a map of the different site locations of ASHES vent field. Each triangle approximates the location of each site. The numbers before each site correlate to the array number used at that site.

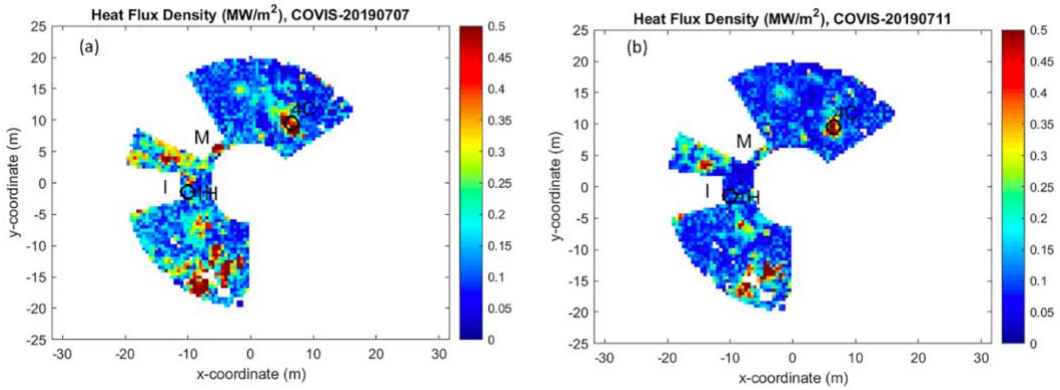

Figure S 3: This figure from Jackson et al. (2022) shows the COVIS heat flux map of ASHES vent field in 1 by 1-meter squares. There are two major shadows in the data caused by the black smokers Inferno and Mushroom, respectively depicted as I and M on the map.